Damage detection under temperature variability using closed-loop mode shapes

B. A. Qadri*, A. S. Kristensen & M. D. Ulriksen

Department of Energy Technology, Aalborg University, 6700 Esbjerg, Denmark

Abstract

The dynamic characteristics of any structural system depend on the temperature. This poses a challenge in vibration-based damage detection, as temperature variability can mask damage-induced shifts in the vibration features. Different means for resolving the issue have been put forth, and two general method types can be distinguished; (*i*) those mitigating the effect of temperature variability on the features and (*ii*) those increasing the sensitivity to damage of the features. The present paper explores the use of features composed of closed-loop (CL) mode shapes, which combine attributes from both method groups by offering adequate sensitivity to damage and robustness to temperature variability. The CL mode shapes are designed using an eigenstructure assignment scheme formulated as a bi-objective optimization problem. The first objective is the reciprocal of the spectral norm of the CL mode shape Jacobian matrix, which is thus to be minimized to maximize the sensitivity to damage. The second objective, whose implementation hinges on the assumptions that temperature variability induces spatially uniform stiffness changes and that homogeneous sensing is employed, is a measure of how much the damping in each of the assigned CL modes deviates from a classical distribution. Since classically damped mode shapes obtained using homogeneous sensing are invariant under spatially uniform stiffness changes, the latter objective is minimized to promote robustness to temperature variability. The designed CL mode shape features can be used in any damage detection method, but in the paper we restrict the use to outlier analysis and assess the merit of the proposed scheme in the context of numerical examples. The damage detection results are compared to findings obtained using cointegration (a well-established method for mitigating the effect of temperature variability), and it is seen how the proposed scheme outperforms the cointegration-based method.

Keywords: damage detection, temperature variability, output feedback, structural health monitoring.

1. Introduction

Using monitored vibration variables to provide an estimate of the health condition of a structure has been recognized as vibration-based damage detection. The monitored variables correspond to features extracted from the vibration response of the structure, while the health condition corresponds to a set of binary states, namely, undamaged and damaged. A pivotal challenge in vibration-based damage detection is to deal with the environmental and operational variabilities observed in the feature set [1, 2]. These variabilities, which are governed by the temperature, wind speed, humidity, excitation level, and so forth, are known to camouflage damaged-induced changes in the feature set and thus deteriorate the damage detectability [3]. Several studies have noted that the temperature constitutes the most influential parameter [4, 5, 6, 7, 8, 9], and therefore we limit this paper to investigate the effect of temperature-induced variability.

For systems exposed to temperature variability, the damage detectability boils down to the ratio between sensitivity to damage (*high is good*) and sensitivity to temperature variability (*high is bad*). There are two ways to improve the ratio; (*i*) by mitigating the effect of temperature variability and (*ii*) by enhancing the sensitivity to damage. Numerous methods have been suggested to mitigate the distortive effect of temperature-induced variability [1, 10]. A common approach is to identify and discriminate between linear sub-spaces carrying information on, respectively, damage and temperature variability. One such method is principal component analysis (PCA), which operates by transforming the feature set into uncorrelated minor and major principal components, so that the major components retain most of the variation present in the features [11]. Yan et al. [12] exemplified the use of PCA to mitigate the effect of temperature variability by projecting their features onto the sub-space of the minor principal components since the major principal components were assumed to retain most of the temperature variability. Other successful application studies concerning PCA can be found in [13, 14].

*Corresponding author. Email: baq@et.aau.dk.

Cointegration, which is a method for analyzing non-stationary signals [15], has also been put forth as a means for mitigating the effect of temperature variability. In this context, the assumptions are that the temperature variability renders the vibration features non-stationary and that the effects of the temperature variability and damage do not couple [16]. Cointegration can then be used to form stationary linear combinations of the non-stationary features, in which the temperature variability is mitigated. The standard procedure in cointegration-based damage detection is to use the most stationary linear combination directly as a damage indicator [16, 17, 18]. Some successful application studies on the use of cointegration for damage detection under temperature variability can be seen in [19, 20].

Regression-based methods have also been suggested to mitigate the effect of temperature variability by explicitly taking into account both the vibration features and covariate information from temperature measurements. Such methods operate by capturing the influence of measured temperature variability on the features by a functional dependence model attained via, for instance, polynomial chaos expansions [21], Gaussian process regression [22, 23], or Bayesian learning [9]. Damage is then detected if the current observation differs significantly from what the regression model predicts. Some documented application studies on the use of regression for damage detection under temperature variability can be seen in [22, 24, 9].

The second option for improving damage detectability, namely, enhancing the sensitivity to damage, can be addressed via structural control schemes. Specifically, closed-loop (CL) systems can be designed by using an eigenstructure assignment scheme, which allows for assignment of eigenvalues and/or eigenvectors (and hence mode shapes) such that these eigencharacteristics exhibit higher sensitivity to damage than the open-loop (OL) counterparts [25, 26, 27]. The concept was introduced to the field of structural damage detection by Ray and Tian [25], who used an eigenstructure assignment scheme to design a feedback controller to enhance the sensitivity to damage of a subset of eigenvalues. The design, which was carried out for a cantilevered beam, resulted in the subset of CL eigenvalues having increased sensitivity to damage compared to the corresponding subset of OL eigenvalues. Jiang et al. [28] showed that if multiple control inputs are available, then further sensitivity enhancement can be attained by assigning both the CL eigenvalues and the associated CL eigenvectors.

The preceding paragraphs summarize some of the extensive research that has been conducted to improve the damage detectability by either mitigating the effect of temperature variability or increasing the sensitivity to damage. One of the remaining issues in this context relates to the relationship between sensitivity to damage and robustness to temperature variability being reciprocal for an unfiltered observation/measurement [29]. It is contended by the authors of the present paper that no feature extraction procedure—despite its level of "intelligence"—can completely decouple the two damage detectability components. In other words, if a method for mitigating the effect of temperature variability is applied, then it will inherently result in a certain loss of information on damage. Likewise, if a control strategy is implemented to enhance the sensitivity to damage of CL eigencharacteristics, then the CL eigensystem will also exhibit increased sensitivity to temperature variability.

In this paper, we propose a new damage detection scheme that addresses (without dissolving) the coupling of the damage detectability components by exploiting the fact that temperature variability is more globally distributed than damage-induced changes. The scheme utilizes designed CL mode shapes as features in a conventional outlier analysis setting with the Mahalanobis distance [30] as discordance measure. The CL mode shapes are designed through eigenvector assignment to offer adequate sensitivity to damage and robustness to temperature variability. The design is carried out as a bi-objective optimization problem, in which the first objective considers the mode shape Jacobian matrix and thus reflects the sensitivity to damage, while the second objective promotes the robustness to temperature variability. In particular, the second objective—which is based on the assumption that temperature variability induces spatially uniform stiffness changes—is formulated as the reciprocal of the condition number of a matrix quantifying the deviation from a classical damping distribution according to Caughey's commutative law [31]. We test the proposed scheme through numerical studies on a frame structure exposed to different levels of temperature variability. In this context, the merit of the proposed scheme is further assessed by comparing its damage detection performance with that of a well-established cointegration-based method [16].

The paper is organized as follows. Section 2 outlines the basics of structural systems theory in OL and presents an illustrative example with a chain system to demonstrate the damage detectability issue often encountered in OL. Section 3 provides a brief description of eigenstructure assignment, while Section 4 outlines the proposed damage detection scheme and returns to the chain system example to show how the scheme can mitigate the damage detectability issue. The numerical damage detection studies with the frame structure exposed to temperature variability are presented in Section 5, and the paper closes with concluding remarks in Section 6.

2. Damage detectability in structural open-loop systems

We consider a structural domain Ω, which is described in OL by the linear, time-invariant (LTI) model

$$M\ddot{x}(t) + C\dot{x}(t) + Kx(t) = B_2u(t), \tag{1}$$

where $\ddot{x}(t)$, $\dot{x}(t)$, $x(t) \in \mathbb{R}^n$ denote the acceleration, velocity, and displacement vectors, $u(t) \in \mathbb{R}^r$ collects the independent inputs that are distributed to Ω by $B_2 \in \mathbb{R}^{n\times r}$, and M, C, $K \in \mathbb{R}^{n\times n}$ are the mass, damping, and stiffness matrices for which it is assumed that $M, C, K \succ 0$.

Definition 1. *The damping model in system* (1) *is denoted classical if $M^{-1}K$ and $M^{-1}C$ commute [31].*

The damping in real structures never strictly complies with the classical distribution given by Definition 1. The majority of all structures will, however, have a subset of well-separated modes, whose damping distribution can be adequately described by the classical damping model [32, 33, 34]. We thus confine the study to classically damped systems and denote the eigenvectors (which are real) and eigenvalues of system (1) by $\phi_j \in \mathbb{R}^n$ and $\lambda_j \in \mathbb{C}$.

By defining the state vector $z(t) = [x(t)^T\ \dot{x}(t)^T]^T \in \mathbb{R}^{2n}$, the output vector $y(t) \in \mathbb{R}^m$, and the system matrices $A_c \in \mathbb{R}^{2n\times 2n}$, $B_c \in \mathbb{R}^{2n\times r}$, and $C_c \in \mathbb{R}^{m\times 2n}$, system (1) can be rewritten into the continuous-time state-space formulation

$$\dot{z}(t) = A_c z(t) + B_c u(t), \tag{2a}$$

$$y(t) = C_c z(t), \tag{2b}$$

where it is assumed that the contribution from the direct feedthrough is zero or subtracted from the measurements. The modal parameters follow from

$$(A_c - \lambda_j I)\psi_j = 0, \qquad \mu_j = C_c \psi_j, \tag{3}$$

where $\psi_j = [\phi_j^T\ \ \phi_j^T\lambda_j]^T \in \mathbb{C}^{2n}$ and $\mu_j \in \mathbb{C}^m$ are, respectively, the eigenvector and mode shape of mode j. Worth of explicit note is that μ_j will be real-valued if the damping is classical and the output sensing is homogeneous (that is, solely displacements, velocities, or accelerations are measured).

2.1. Modal parameters as damage detection features

LTI systems can be fully described by means of the modal parameters, and therefore it makes sense to discuss damage detectability for structural systems on the basis of these parameters. Assumptions 1 and 2 are prerequisites for the discussion.

Assumption 1. *Temperature variability induces spatially uniform stiffness changes, which perturb the stiffness of system* (1) *from K to αK with $\alpha \in \mathbb{R}_{>0}$.*

Assumption 2. *Damage is local and yields a stiffness perturbation $\Delta K \in \mathbb{R}^{n\times n}$ for which rank$(\Delta K) < n$.*

Proposition 1. *Assume that system* (1) *is classically damped and let (λ_j, ϕ_j) be an eigenpair of the system. If the stiffness is perturbed in accordance with Assumption 1, then $(\tilde{\lambda}_j, \phi_j)$ is an eigenpair of the perturbed system with $|\tilde{\lambda}_j|^2 = \alpha|\lambda_j|^2$.*

Proof. The undamped eigenvalue problem for the perturbed system can be written as

$$\left(\alpha K - |\tilde{\lambda}_j|^2 M\right)\tilde{\phi}_j = \alpha\left(K - \frac{|\tilde{\lambda}_j|^2}{\alpha} M\right)\tilde{\phi}_j = 0, \tag{4}$$

so Null$\left(K - \frac{|\tilde{\lambda}_j|^2}{\alpha} M\right) \neq \emptyset$ if and only if $|\tilde{\lambda}_j|^2 = \alpha|\lambda_j|^2$. It follows that $\phi_j \in$ Null$\left(\alpha K - |\tilde{\lambda}_j|^2 M\right)$, leading to the assertion. □

As shown in Proposition 1, the eigenvalues of a classically damped LTI system are affected by spatially uniform stiffness changes; with the undamped eigenfrequencies changing linearly by a factor of α. The associated mode shapes specified in (3) are, however, invariant to the uniform stiffness variability when homogeneous output sensing is employed. We exemplify the use of system eigenvalues and mode shapes as damage indicators under temperature variability in Subsection 2.2.

2.2. Illustrative example

The issue of temperature variability is demonstrated in the context of the chain system depicted in Fig. 1. The chain system, which is classically damped with 5 % damping in each mode in the undamaged state presented in Fig. 1, is affected by an imposed temperature field yielding a system stiffness of αK, where K is the nominal stiffness matrix according to Fig. 1 and $\alpha \in [0.97, 1]$. An impulse force is applied to the sixth degree of freedom (DOF), and the output is taken as the displacement response measured at the first and second DOF. The output, which is captured with a sampling frequency of 150 Hz, is contaminated with 2 % white Gaussian noise.

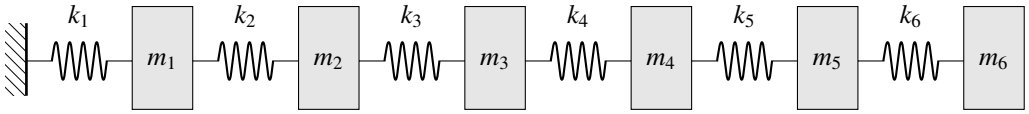

Fig. 1: 6-DOF chain system with $k_i = 1000$ and $m_i = 2$ in consistent units and a classical damping distribution with 5 % critical damping in each mode.

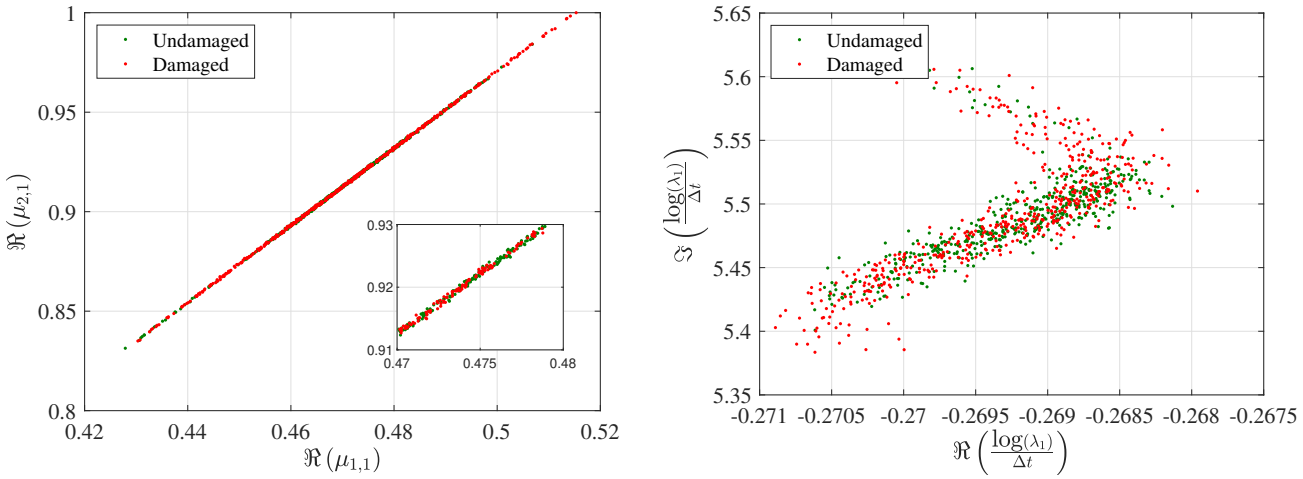

(a) **(b)**

Fig. 2: Estimated eigencharacteristics of the first OL mode of the chain system with (a) showing the mode shape and (b) the eigenvalue for both structural states.

The chain system is analyzed in its undamaged structural state and in a damaged structural state where the stiffness of the third spring is reduced by 0.2 %. Both the mass and the damping are assumed invariant to the introduced damage. A total of 1000 realizations are simulated, with the first 500 realizations being from the undamaged state and the remaining 500 from the damaged state. We employ a stochastic sub-space identification (SSI) method [35] to estimate the modal parameters for each realization, and the results can be seen in Figs. 2a and 2b. Evidently, no clear decision boundary arises for neither the mode shape estimates nor the eigenvalue estimates when damage is introduced. The extracted eigenvalues are correlated with the temperature variability, while the mode shapes, in accordance with Eq. (4), are invariant to the variability. Despite the invariance, the damage detectability offered by the mode shape is insufficient since its sensitivity to damage is too low.

3. Output feedback

We introduce a temporal discretization of system (2) under the assumption that the input is delivered with a zero-order-hold (ZOH) with an inter-sample time of Δt. The discretization yields

$$z_{k+1} = A_d z_k + B_d u_k, \tag{5a}$$

$$y_k = C_d z_k, \tag{5b}$$

with the system matrices $A_d = e^{A_c \Delta t}$, $B_d = A_c^{-1}(A_d - I)B_c$, and $C_d = C_c$. Since A_d is square, it follows that $A_d = e^{A_c \Delta t} = \sum_{i=0}^{\infty} \frac{1}{i!} A_c^i (\Delta t)^i$. It can thus be readily shown that the eigenvectors and eigenvalues of A_d equal ψ_j and $e^{\lambda_j \Delta t}$, where (ψ_j, λ_j) is the continuous-time eigenpair defined in (3).

We apply static output feedback to the OL system (5a) of the type

$$u_k = -G y_k, \tag{6}$$

where $G \in \mathbb{R}^{r \times m}$ is the controller gain. Substituting (6) in (5a) gives the system of CL state equations

$$z_{k+1} = (A_d - B_d G C_d) z_k = \bar{A}_d z_k, \tag{7}$$

with $\bar{A}_d \in \mathbb{C}^{2n\times 2n}$ being the discrete-time CL state matrix.

Lemma 1. *Let C^{dis}, C^{vel}, and C^{acc} denote the output selection matrices for displacement, velocity, and acceleration measurements, then the CL stiffness and damping matrices of system* (7) *are given as*

- $\bar{K} = K + B_2GC^{dis}$ *and* $\bar{C} = C$ *for homogeneous displacement sensing,*
- $\bar{K} = K$ *and* $\bar{C} = C + B_2GC^{vel}$ *for homogeneous velocity sensing, and*
- $\bar{K} = (I - B_2GC^{acc}M^{-1})K$ *and* $\bar{C} = (I - B_2GC^{acc}M^{-1})C$ *for homogeneous acceleration sensing,*

while the CL mass matrix equals the OL mass matrix independently of the sensing type.

Proof. The proof follows directly by transforming (7) to continuous time. □

Theorem 1. *If at least one of the two conditions $m < n$ and $r < n$ holds for system* (7) *under homogeneous sensing, then the system's damping, as defined in Lemma 1, is non-classical for all $G \neq 0$.*

Proof. See the proof by Ulriksen [36]. □

From Theorem 1, it follows that in the typical case where $m << n$ and $r << n$, the CL system damping will not follow a classical distribution and the CL mode shapes will thus depend on the temperature.

3.1. Eigenvalue and eigenvector assignment

Let $\Lambda = \{\bar{\lambda}_1, \ldots, \bar{\lambda}_p, \bar{\lambda}_1^*, \ldots, \bar{\lambda}_p^*\}$ be a set of $2p$ discrete-time eigenvalues (with superscript $*$ denoting complex conjugate) to be assigned for system (7), then it follows for $\bar{\lambda}_j \in \Lambda$ that

$$(A_d - B_dGC_d)\,\bar{\psi}_j = \bar{\lambda}_j\bar{\psi}_j, \tag{8}$$

or, in partitioned form,

$$\begin{bmatrix} A_d - \bar{\lambda}_j I & -B_d \end{bmatrix} \begin{Bmatrix} \bar{\psi}_j \\ b_j \end{Bmatrix} = 0, \tag{9}$$

where $b_j = GC_d\bar{\psi}_j \in \mathbb{C}^r$ and $\bar{\psi}_j \in \mathbb{C}^{2n}$ are extracted from the null space of $\begin{bmatrix} A_d - \bar{\lambda}_j I & -B_d \end{bmatrix}$. If the nullity is more than one, then b_j and $\bar{\psi}_j$ can be taken as combinations of the null vectors. Collecting b_j and $\bar{\psi}_j$ such that $\Psi = C_d \begin{bmatrix} \bar{\psi}_1 \ldots \bar{\psi}_{2p} \end{bmatrix} \in \mathbb{C}^{m\times 2p}$ and $\Gamma = \begin{bmatrix} b_1 \ldots b_{2p} \end{bmatrix} \in \mathbb{C}^{r\times 2p}$, it follows that

$$G\Psi = \Gamma, \tag{10}$$

such that the gain can be computed by inversion when Ψ has full rank and the number of assigned eigenvalues, $2p$, equals the number of outputs, m. Since transposition does not change the eigenvalues, one can also operate with left-side eigenvectors and assign r eigenvalues.

If $2p > m$, (10) becomes overdetermined and the computed gain may not realize the assigned eigencharacteristics. One way of mitigating this issue is to define $\hat{\Psi} = C_d \begin{bmatrix} \bar{\psi}_1 \ldots \bar{\psi}_{2n} \end{bmatrix} \in \mathbb{C}^{m\times 2n}$ and $\hat{\Gamma} = \begin{bmatrix} b_1 \ldots b_{2n} \end{bmatrix} \in \mathbb{C}^{r\times 2n}$ and then, under the assumption that $p < n$, introduce a weighted least squares solution as

$$G = \hat{\Gamma}W\hat{\Psi}^H\left(\hat{\Psi}W\hat{\Psi}^H\right)^{-1}, \tag{11}$$

where the superscript H denotes the conjugate transpose and $W = \mathrm{diag}(\eta_1, \ldots, \eta_{2p}, 1, \ldots, 1) \in \mathbb{R}^{2n\times 2n}$ is a diagonal weighting matrix; with η_i denoting the weights, which are taken such $\eta_i = \eta$. As pointed out by Bernal and Ulriksen [26], good performance can be obtained for a wide range of η-values, thus no "fine-tuning" is required.

3.2. Mode shape sensitivities

Let $\bar{C}_d$ be the CL output matrix, then the jth CL mode shape follows as $\bar{\mu}_j = \bar{C}_d \bar{\psi}_j$. The sensitivity of $\bar{\mu}_j$ with respect to a structural parameter ϵ is thus given by

$$\frac{\partial \bar{\mu}_j}{\partial \epsilon} = \frac{\partial \bar{C}_d}{\partial \epsilon} \bar{\psi}_j + \bar{C}_d \frac{\partial \bar{\psi}_j}{\partial \epsilon}, \tag{12}$$

where $\partial \bar{C}_d / \partial \epsilon$ is easily computed for the particular sensing/measurement type, while $\partial \psi_j / \partial \epsilon$ is derived by taking the partial derivative with respect to ϵ on both sides of (8). Hereby,

$$\frac{\partial \bar{A}_d}{\partial \epsilon} \bar{\psi}_j + \bar{A}_d \frac{\partial \bar{\psi}_j}{\partial \epsilon} = \frac{\partial \bar{\lambda}_j}{\partial \epsilon} \bar{\psi}_j + \bar{\lambda}_j \frac{\partial \bar{\psi}_j}{\partial \epsilon} \tag{13}$$

such

$$\left(\bar{A}_d - \bar{\lambda}_j I\right) \frac{\partial \bar{\psi}_j}{\partial \epsilon} = \left(\frac{\partial \bar{\lambda}_j}{\partial \epsilon} I - \frac{\partial \bar{A}_d}{\partial \epsilon}\right) \bar{\psi}_j, \tag{14}$$

which can be solved using Nelson's method [37]. We note that the method calls for the computation of the eigenvalue sensitivity, $\partial \bar{\lambda}_j / \partial \epsilon$, which can be found from (13). Furthermore, the method requires the partial derivative of the CL state matrix, which writes

$$\frac{\partial \bar{A}_d}{\partial \epsilon} = \frac{\partial A_d}{\partial \epsilon} - \frac{\partial B_d}{\partial \epsilon} G C_d - B_d G \frac{\partial C_d}{\partial \epsilon}, \tag{15}$$

with

$$\frac{\partial B_d}{\partial \epsilon} = A_c^{-1} \left(\frac{\partial A_d}{\partial \epsilon} B_c + A_d \frac{\partial B_c}{\partial \epsilon} - \frac{\partial B_c}{\partial \epsilon} - \frac{\partial A_c}{\partial \epsilon} B_d \right). \tag{16}$$

Thus, substitution of (16) into (15) yields

$$\frac{\partial \bar{A}_d}{\partial \epsilon} = \frac{\partial A_d}{\partial \epsilon} - A_c^{-1} \left(\frac{\partial A_d}{\partial \epsilon} B_c + (A_d - I) \frac{\partial B_c}{\partial \epsilon} - \frac{\partial A_c}{\partial \epsilon} B_d \right) G C_d - B_d G \frac{\partial C_d}{\partial \epsilon}, \tag{17}$$

where the partial derivative of A_d with respect to the structural parameter can be taken as the complex step approximation [38]

$$\frac{\partial A_d}{\partial \epsilon} = \lim_{h \to 0} \Im \left(\frac{e^{\left(A_c + \frac{\partial A_c}{\partial \epsilon} hi\right) \Delta t}}{h} \right). \tag{18}$$

4. Damage detection using closed-loop mode shapes

The low sensitivity to damage of OL mode shapes, which is exemplified in Subsection 2.2, is well-known and documented in numerous application studies [2]. In the present section, we propose a scheme for outlier analysis-based damage detection with features composed of CL mode shapes, which are designed to offer enhanced sensitivity to damage while retaining an adequate robustness to temperature variability.

4.1. Optimal gain design

Feedback gains are designed in a bi-objective optimization setting such that each of the resulting CL systems has one mode shape assigned to exhibit an adequate trade-off between sensitivity to damage and robustness to temperature variability. Specifically, q modes are selected from the OL system (typically based on the identifiability of these modes), and then q gains are designed such that G_i assigns the mode shape of the ith mode of the selected subset. The gain designs are carried out by use of the eigenstructure assignment scheme outlined in Subsection 3.1, with the aid of a *design model* of the undamaged structural system in question.

4.1.1. Objective function 1: Sensitivity to damage

The sensitivity to damage of a CL mode shape, $\bar{\mu}_i$, is given by (12) when ϵ is taken as a stiffness-related parameter. For each of the q mode shapes to be assigned, we establish the Jacobian matrix

$$\mathcal{S}_i = \begin{bmatrix} \frac{\partial \bar{\mu}_{1i}}{\partial \epsilon_1} & \frac{\partial \bar{\mu}_{1i}}{\partial \epsilon_2} & \cdots & \frac{\partial \bar{\mu}_{1i}}{\partial \epsilon_n} \\ \frac{\partial \bar{\mu}_{2i}}{\partial \epsilon_1} & \frac{\partial \bar{\mu}_{2i}}{\partial \epsilon_2} & \cdots & \frac{\partial \bar{\mu}_{2i}}{\partial \epsilon_n} \\ \vdots & \vdots & \ddots & \vdots \\ \frac{\partial \bar{\mu}_{mi}}{\partial \epsilon_1} & \frac{\partial \bar{\mu}_{mi}}{\partial \epsilon_2} & \cdots & \frac{\partial \bar{\mu}_{mi}}{\partial \epsilon_n} \end{bmatrix}, \tag{19}$$

where $\bar{\mu}_{ki}$ denotes the kth entry in the ith mode shape to be assigned and ϵ_j is the jth stiffness-related parameter. We define the cost function

$$\mathcal{F}_1^{(i)} = \frac{1}{\|\mathcal{S}_i\|_2}, \tag{20}$$

which must be minimized in order to maximize (in a spectral norm-sense) the sensitivity to damage of the ith assigned CL mode shape. With $\mathcal{S}_i^{\mathrm{OL}}$ denoting the Jacobian of the corresponding OL mode shape, the condition $\|\mathcal{S}_i\|_2 > \|\mathcal{S}_i^{\mathrm{OL}}\|_2$ must be fulfilled. Compliance with the condition will obviously *not* result in $\left|\partial \bar{\mu}_{ki}/\partial \epsilon_j\right| > \left|\partial \mu_{ki}/\partial \epsilon_j\right|$ for all $k = 1, \ldots, m$, $j = 1, \ldots, n$, so the use of multiple gains (that is, $q > 1$) is encouraged to promote adequate sensitivity to any local damage of interest.

4.1.2. Objective function 2: Robustness to temperature variability

According to Theorem 1, CL systems are, in general, non-classically damped, so the CL mode shapes are not invariant to uniform temperature variability. In order to promote robustness to temperature variability, we introduce a second objective function that quantifies the extent to which the damping in each of the assigned CL modes deviates from a classical distribution. In particular, let ρ denote the condition number operator, then the second objective function is defined as

$$\mathcal{F}_2^{(i)} = \frac{1}{\rho\left[\Re\left(\bar{\mu}_i\right) \quad \Im\left(\bar{\mu}_i\right)\right]}, \tag{21}$$

where $\rho\left[\Re\left(\bar{\mu}_i\right) \quad \Im\left(\bar{\mu}_i\right)\right] = \infty$ in the limit with a classically damped/undamped mode shape. Hence, $\mathcal{F}_2^{(i)}$ is to be minimized in order to promote robustness to temperature variability.

4.1.3. Optimization formulation

Let $\mathcal{G} \subset \mathbb{R}^{r \times m}$ be the space of feasible gains—that is, gains that the r input controllers can deliver—and let $\bar{\zeta}_i$ and $\bar{\omega}_i$ denote the CL damping ratio[2] and damped eigenfrequency associated with the mode shape being assigned. Then, the design of each gain is conducted on the basis of the following bi-objective optimization problem:

$$\begin{aligned} \hat{G}_i = \underset{G_i \in \mathcal{G}}{\arg\min} \quad & \left(\mathcal{F}_1^{(i)}, \mathcal{F}_2^{(i)}\right) \\ \text{subject to} \quad & \forall j \in [1, 2n] : \|\bar{\lambda}_j\| < 1, \\ & 0 < \bar{\zeta}_i \leq \bar{\zeta}_i^U, \\ & \bar{\omega}_i^L \leq \bar{\omega}_i \leq \bar{\omega}_i^U, \end{aligned} \tag{22}$$

in which explicit reference to any structural state is omitted, as the constraints must be complied with both prior and posterior to the occurrence of damage. Obviously, one does not know the damaged state, so a maximum allowable damage extent is defined and the design model is perturbed accordingly to ascertain the compliance with the constraints. The first constraint in (22) ensures system stability, while the second and third constraints are defined such that the particular CL eigenvalue of interest is identifiable through system identification and in the vicinity of the corresponding OL eigenvalue. In particular, $\bar{\zeta}_i^U$

[2]For a non-classically damped mode, the notion of an associated damping ratio does no longer strictly apply. However, we still use the notion in accordance with the classically damped formulation.

is an upper bound on the CL damping ratio and $\bar{\omega}_i^L$ and $\bar{\omega}_i^U$ bound the associated CL damped eigenfrequency. The CL mode shape assigned by use of $\hat{G}_i$ is denoted $\bar{\mu}_i(\hat{G}_i)$.

Problem (22) can be solved by either (*i*) transforming it into two single-criterion subproblems using, for example, the Weighted Sum Method [39] or the ϵ-Constraint Method [40] or (*ii*) searching for the Pareto-optimal set using, for example, multi-objective evolutionary algorithms [41]. In the illustrative example in Subsection 4.3 and the application example in Section 5, we will use the Weighted Sum Method to solve (22).

4.2. Proposed damage detection scheme

As noted in Subsection 4.1, $\bar{\mu}_i(\hat{G}_i) \in \mathbb{C}^m$ is the assigned mode shape in the CL system with the optimal gain $\hat{G}_i$. If q gain designs are carried out, then the resulting q assigned mode shapes are gathered in

$$\Xi = \begin{bmatrix} \bar{\mu}_1(\hat{G}_1)^T & \dots & \bar{\mu}_q(\hat{G}_q)^T \end{bmatrix}^T \in \mathbb{C}^{mq}, \tag{23}$$

which constitutes the feature vector used in the proposed damage detection scheme. A series of $N_{\text{tr}} \geq mq$ realizations of (23) are extracted in the undamaged structural state and gathered in the matrix $\Sigma = \begin{bmatrix} \Xi_1^{\text{tr}} & \Xi_2^{\text{tr}} & \dots & \Xi_{N_{\text{tr}}}^{\text{tr}} \end{bmatrix} \in \mathbb{C}^{mq \times N_{\text{tr}}}$, which is used to train a baseline model. The baseline model is composed of the mean of Σ, denoted $\nu_\Sigma \in \mathbb{C}^{mq}$, and the cross-covariance of Σ, denoted $\Delta_\Sigma \in \mathbb{C}^{mq \times mq}$.

Let Ξ_i^{te} be the ith feature vector realization from the current, potentially damaged state to be tested, then the Mahalanobis distance

$$D_i^2\left(\Xi_i^{\text{te}}, \Sigma\right) = \left(\Xi_i^{\text{te}} - \nu_\Sigma\right)^H \Delta_\Sigma^{-1} \left(\Xi_i^{\text{te}} - \nu_\Sigma\right) \tag{24}$$

is employed to quantify the discordance between Ξ_i^{te} and the baseline model. D_i^2 thus constitutes the damage index from which inferences regarding the structural state are made. Specifically, if $\mathcal{D}$ is the selected threshold, then $D_i^2 \leq \mathcal{D}$ implies that the structure is undamaged, while $D_i^2 > \mathcal{D}$ implies that the structure is damaged.

4.3. Illustrative example

We return to the chain system depicted in Fig. 1 and retain the setup with noise-contaminated displacement output captured at the first and second DOF with a sampling frequency of 150 Hz. An impulse force is applied to the sixth DOF to excite the structure and the actuator delivering the feedback is positioned at the fourth DOF. The gain is designed by placing the first CL eigenvector in accordance with (22). In this context, we set $\eta = 1000$ and $\bar{\zeta}_i^U = 0.08$. With the attained gain, we conduct 500 CL simulations in both the undamaged and the damaged state and obtain the estimated CL eigencharacteristics seen in Fig. 3. Evidently, the eigenvalue estimates appear to be more affected by the temperature variability than the OL counterparts, see

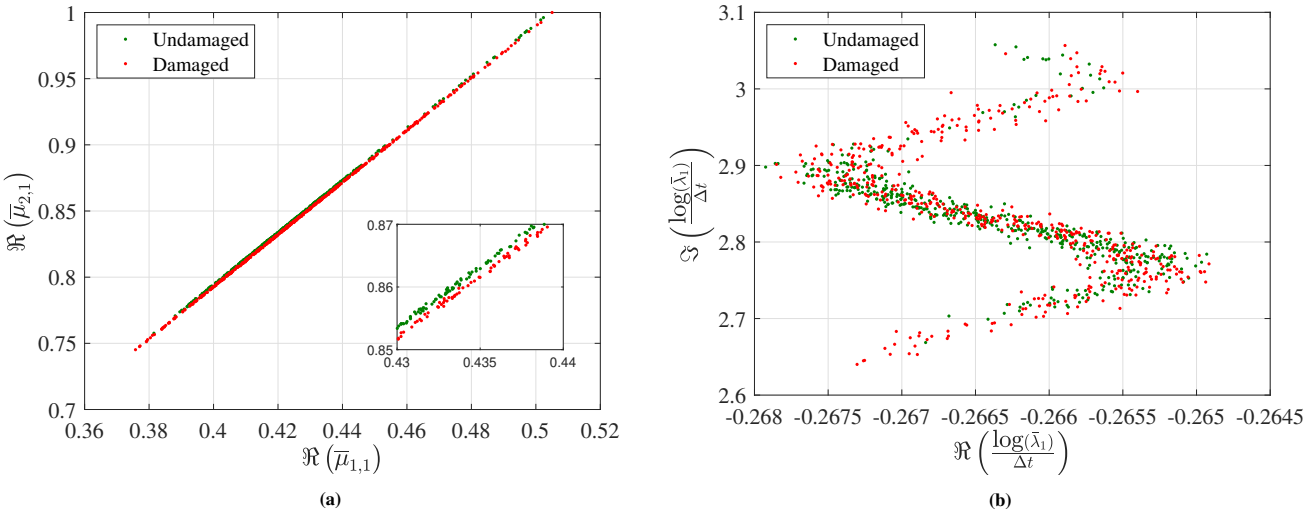

Fig. 3: Estimated eigencharacteristics of the first CL mode of the chain system with (a) showing the mode shape and (b) the continuous-time eigenvalue for both structural states.

Fig. 2b, and no clear decision boundary exists between the CL realizations from the two structural states. The CL mode shape estimates are, however, clustered according to the structural states with a clear decision boundary in between. Compared to the OL mode shapes, see Fig. 2a, we have thus gained some sensitivity to damage at the expense of strict invariance to the temperature variability.

5. Application example

We consider the 2-story frame structure depicted in Fig. 4 and use the term *simulation models* to refer to the models (of the undamaged and damaged structural states) used to simulate experiments. The design model and the undamaged simulation model are throughout assumed identical, thus no model errors are introduced. The structure is modeled using 16 two-dimensional Euler-Bernoulli beam elements with a material model corresponding to structural steel. Classical damping is assumed in OL such that each mode has a damping ratio of 5 % in the undamaged OL state. An impulse excitation, v_k, is applied to the frame structure, and an actuator delivering displacement output feedback, u_k, is positioned between floor 1 and 2 as depicted in Fig. 4. The displacement response, y_k^i, is captured at floor 1 and between floors 1 and 2 with a sampling frequency of 13 kHz. The displacements are contaminated with 2 % white Gaussian noise, and the structure is simultaneously exposed to a spatially uniform temperature variability for which $\alpha \in [0.97, 1]$ in accordance with Assumption 1. Damage is emulated by reducing the Young's modulus of a single element by 3 %. We confine the study to two damage cases; namely, case 1 in which the stiffness of element 1 is reduced and case 2 in which the stiffness of element 7 is reduced.

5.1. Feature design and extraction

The design model is used for designing two gains in accordance with (22). The first gain is designed by assigning the mode shape of the first CL mode, while the second gain is designed by assigning the mode shape of the second CL mode. With reference to (22), we set $\bar{\zeta}_1^U = \bar{\zeta}_2^U = 0.1$ (hence allowing up to 10 % critical damping) and $0.5\omega_i \leq \bar{\omega}_i \leq 2\omega_i$, where ω_i is the corresponding OL eigenfrequency. The frequency bounds are selected to ensure that the assigned eigenvalues are identifiable and that they do not become closely spaced with the other frequencies in the eigenspectra. A constraint with respect to the maximum allowable damage is defined such that we permit up to 20 % damage at each element, and in each gain design the eigenvalue associated with the mode to be assigned is weighted such that $\eta = 7500$. By use of the Weighted Sum Method, we solve (22) for the two gain designs and obtain the findings presented in Tb. 1. It follows from the ratios $\mathcal{F}_1^{\mathrm{OL}}/\mathcal{F}_1^{(i)}$, where $\mathcal{F}_1^{\mathrm{OL}}$ is the inverse of the spectral norm of the OL mode shape Jacobian, that we (in a spectral norm-sense) gain 4.5 and 9.3 times more mode shape sensitivity in the two assigned modes compared to the corresponding OL modes.

In the damage detection analysis, the following feature sets are explored: *(i)* the first mode shape (designed by using the first gain), *(ii)* the second mode shape (designed by using the second gain), and *(iii)* the two mode shapes stacked. The features

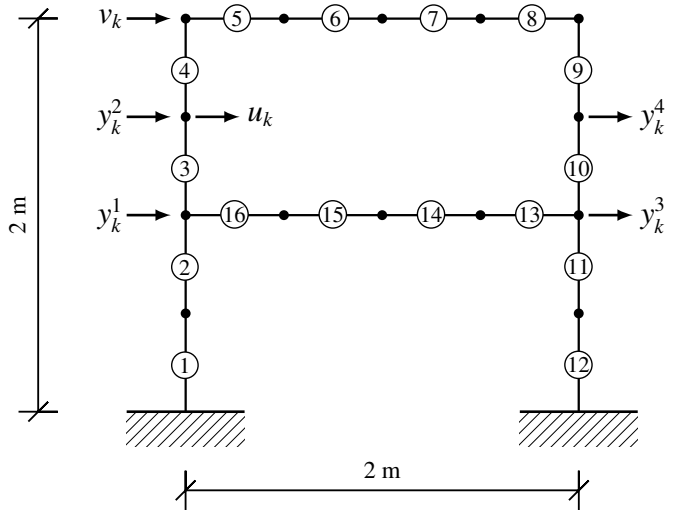

Fig. 4: 2-story frame structure model with an exogenous input, v_k, a control input, u_k, and four displacement outputs, y_k^i. The circle numbering denotes the particular element number.

Tb. 1: Gain design results obtained using (22) with $\zeta_i^U = 0.08$ and $0.5\omega_i \leq \bar{\omega}_i \leq 2\omega_i$, where ω_i is the corresponding OL eigenfrequency.

Gain design	Cost function values[a]	Assigned CL mode shape[b]	Associated eigenvalue[c]
1	$\frac{\mathcal{F}_1^{\mathrm{OL}}}{\mathcal{F}_1^{(1)}} = 4.534,\ \mathcal{F}_2^{(1)} = 1.462 \cdot 10^{-5}$	$\frac{\bar{\mu}_1(\hat{G}_1)}{\left\|\bar{\mu}_1(\hat{G}_1)\right\|_2} = \begin{bmatrix} 0.371 + 0.000\,j \\ 0.603 + 0.000\,j \\ 0.602 + 0.000\,j \\ 0.371 + 0.000\,j \end{bmatrix}$	$\frac{\log(\bar{\lambda}_1(\hat{G}_1))}{\Delta t} = -7.880 + 155.598\,j$
2	$\frac{\mathcal{F}_1^{\mathrm{OL}}}{\mathcal{F}_1^{(2)}} = 9.278,\ \mathcal{F}_2^{(2)} = 0.025$	$\frac{\bar{\mu}_2(\hat{G}_2)}{\left\|\bar{\mu}_2(\hat{G}_2)\right\|_2} = \begin{bmatrix} 0.336 + 0.000\,j \\ 0.524 - 0.004\,j \\ 0.703 + 0.032\,j \\ 0.344 + 0.002\,j \end{bmatrix}$	$\frac{\log(\bar{\lambda}_2(\hat{G}_2))}{\Delta t} = -25.747 + 297.662\,j$

[a] $\mathcal{F}_1^{\mathrm{OL}}$ is the inverse of the spectral norm of the OL mode shape Jacobian and $\mathcal{F}_2^{\mathrm{OL}} = 0$.
[b] The OL eigenvectors of modes 1 and 2 are $[0.370\ \ 0.602\ \ 0.602\ \ 0.370]^T$ and $[0.673\ \ 0.218\ \ 0.218\ \ 0.673]^T$.
[c] The OL eigenvalues of modes 1 and 2 are $-7.877 + 157.345\,j$ and $-27.713 + 553.574\,j$.

are computed by use of the SSI method. We extract 300 realizations from the undamaged state and 100 realizations from each of the two damaged states. The Mahalanobis distance (24) is used for outlier analysis, and we establish the training model based on 150 realizations from the undamaged state, while the remaining 150 realizations from this structural state are used for testing along with the 100 realizations from each of the damaged states.

5.2. Damage detection results

Figs. 5a to 5c display the Mahalanobis distances for damage case 1 obtained using the three different feature sets, while the corresponding results for damage case 2 are seen in Figs. 5d to 5f. From Figs. 5a and 5c, we can see that good performance is obtained when using feature set 1 (that is, the first CL mode shape) and feature set 3 (that is, the combination of CL mode shapes 1 and 2) since a clear decision boundary between the damaged and undamaged states is present. The results in Fig. 5b

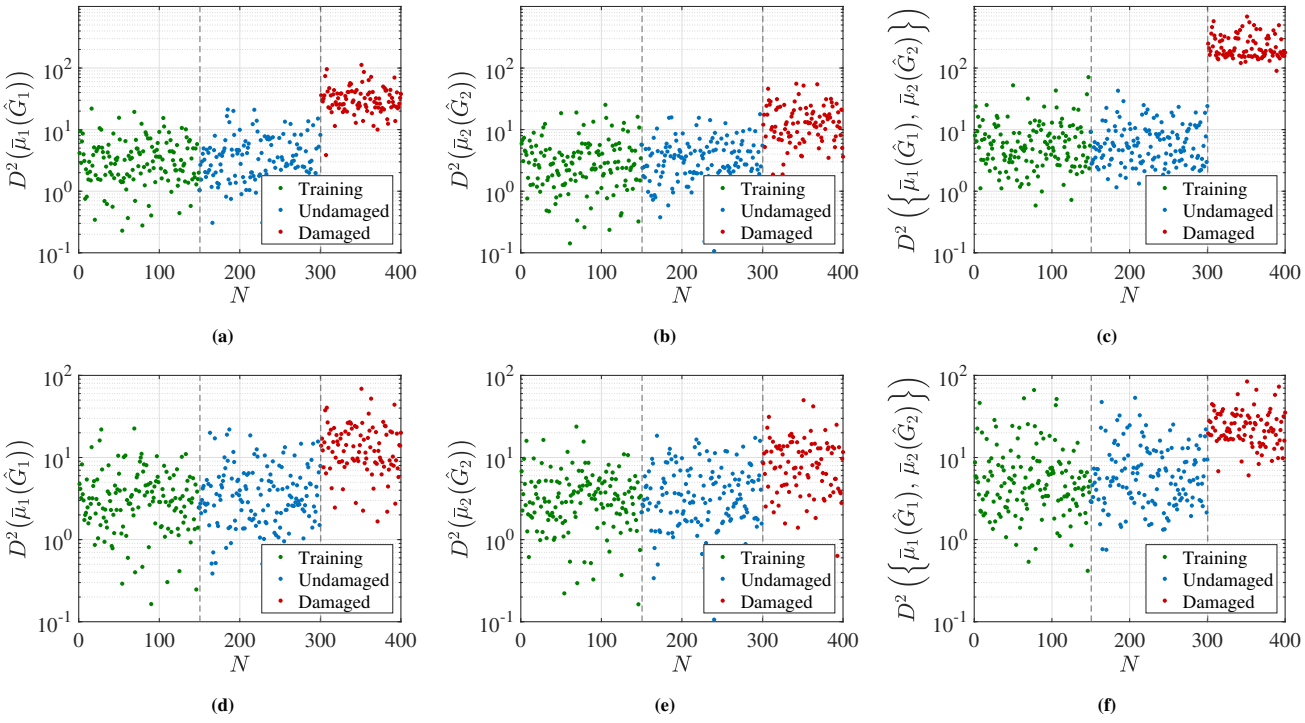

Fig. 5: Mahalanobis distances of features $\bar{\mu}_1(\hat{G}_1)$, $\bar{\mu}_2(\hat{G}_2)$, and $\left\{\bar{\mu}_1(\hat{G}_1), \bar{\mu}_2(\hat{G}_2)\right\}$ in (a)–(c) damage case 1 and (d)–(f) damage case 2.

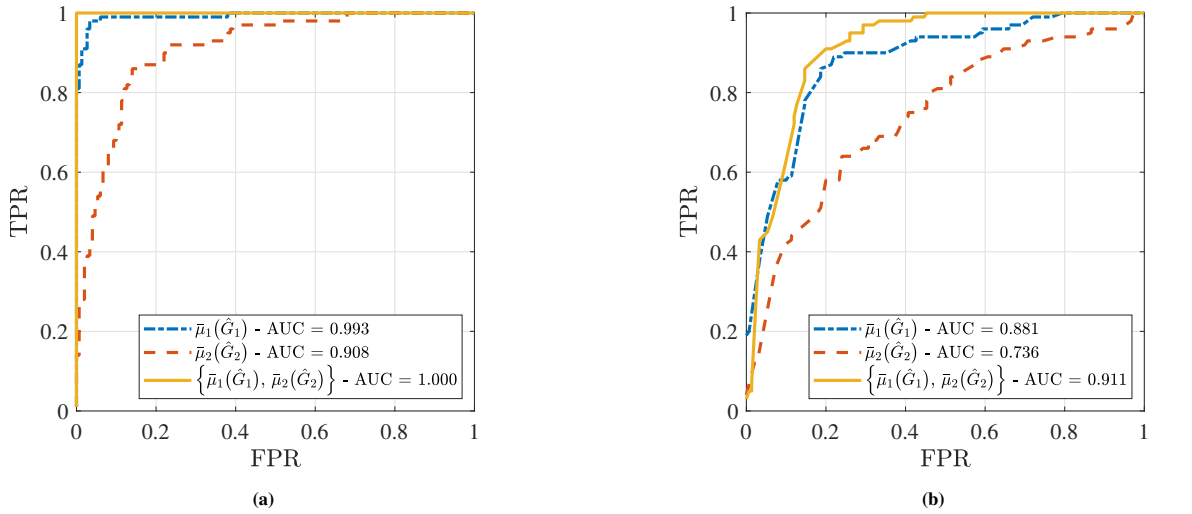

Fig. 6: ROC curves and AUC values attained when using $\bar{\mu}_1(\hat{G}_1)$, $\bar{\mu}_2(\hat{G}_2)$, and $\{\bar{\mu}_1(\hat{G}_1), \bar{\mu}_2(\hat{G}_2)\}$ as features in (a) damage case 1 and (b) damage case 2.

Tb. 2: Summary of the detection performances attained for damage cases 1 and 2 when using $\bar{\mu}_1(\hat{G}_1)$, $\bar{\mu}_2(\hat{G}_2)$, and $\{\bar{\mu}_1(\hat{G}_1), \bar{\mu}_2(\hat{G}_2)\}$ as feature vectors.

Feature vector, Ξ	Damage case 1				Damage case 2			
	AUC	TPR	FPR	Acc.	AUC	TPR	FPR	Acc.
$\bar{\mu}_1(\hat{G}_1)$	0.993	0.980	0.033	0.972	0.881	0.860	0.187	0.832
$\bar{\mu}_2(\hat{G}_2)$	0.908	0.860	0.140	0.860	0.736	0.580	0.200	0.712
$\{\bar{\mu}_1(\hat{G}_1), \bar{\mu}_2(\hat{G}_2)\}$	1.000	1.000	0.000	1.000	0.911	0.860	0.147	0.856

display a somewhat fuzzy decision boundary, thus the damage detectability provided by mode shape 2 is lower than the one provided by mode shape 1. As seen in Figs. 5d and 5e, the same tendency is observed in damage case 2, where mode shape 2 provides insufficient damage detectability. A clear decision boundary is, as seen in Fig. 5f, only attained when both mode shapes are used in the feature set. The observations are supported by the receiver operating characteristic (ROC) curve for each damage case, see Figs. 6a and 6b. The performance in each damage case is summarized in Tb. 2 on the basis of the area under the ROC curve (AUC), the true positive rate (TPR), the false positive rate (FPR), and the accuracy (Acc) [42].

5.2.1. The effect of the temperature variability level

We examine the effect of the temperature variability level on the damage detection performance of the proposed scheme. We do this in the context of damage case 2 using $\{\bar{\mu}_1(\hat{G}_1), \bar{\mu}_2(\hat{G}_2)\}$ as the feature vector. Four scenarios are explored, namely, 1 %, 3 %, 5 %, and 10 % uniform stiffness variability, where it is noted that the setting with 3 % has already been documented. The attained ROC curves are presented in Fig. 7, where it can be seen that the AUC, as expected, increases as the temperature variability decreases. The performance is summarized in Tb. 3 by the AUC, TPR, FPR, and Acc. To this end, the results confirm that the designed mode shape features—albeit not invariant under temperature variability—display adequate robustness to temperature variability.

Tb. 3: Summary of the detection performances attained at different temperature variability levels for damage case 2 with $\{\bar{\mu}_1(\hat{G}_1), \bar{\mu}_2(\hat{G}_2)\}$ as feature vectors.

Temperature variability	AUC	TPR	FPR	Acc.
1 %	0.972	0.910	0.053	0.932
3 %	0.911	0.860	0.147	0.856
5 %	0.853	0.780	0.207	0.789
10 %	0.700	0.590	0.280	0.668

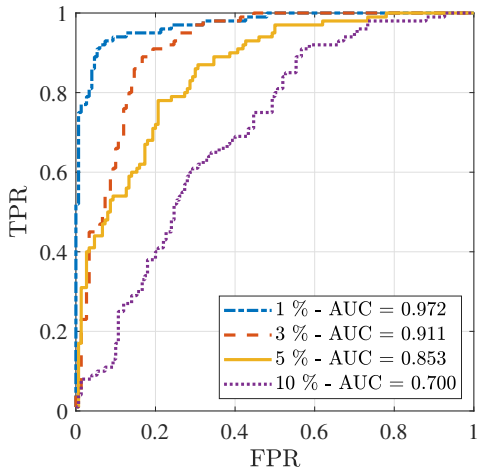

Fig. 7: ROC curves for different temperature variability levels for damage case 2 with $\left\{\bar{\mu}_1(\hat{G}_1), \bar{\mu}_2(\hat{G}_2)\right\}$ as feature .

5.2.2. Comparison with an existing EOV mitigation method

The proposed CL scheme is compared to a well-established cointegration-based method [16] in the context of damage case 2 with a temperature variability of 3 %. The feature set used in the cointegration is composed of the first and second OL eigenvalues. The SSI method is employed to extract the features, which are gathered in $\mathcal{H} = [\lambda_1 \;\; \lambda_2]$. The columns in $\mathcal{H}$ are said to be cointegrated if a linear combination of them is stationary. Given that this stationary combination/residual exists, it can be computed as

$$\mathcal{Z} = \beta^T \mathcal{H}, \tag{25}$$

where β is the so-called cointegration vector. When utilizing cointegration, two main conditions must be satisfied; (*i*) the series of variables, found in the columns of $\mathcal{H}$, must be integrated with the same order (i.e., the columns must have the same "degree of non-stationarity" [16]) and (*ii*) the series must share common trends. Assuming the aforementioned conditions are satisfied, the Johanson procedure [43] can be employed to compute the cointegration vector.

The first step in the Johansen procedure is to fit a series of training realizations, gathered in $\mathcal{H}^{\text{tr}}$, to a c-order vector error correction model (VECM) of the form [16]

$$\Delta\mathcal{H}_b^{\text{tr}} = \upsilon\beta^T\mathcal{H}_{b-1}^{\text{tr}} + \sum_{i=1}^{c-1} \mathcal{P}_i \Delta\mathcal{H}_{b-i}^{\text{tr}} + \mathcal{E}_b, \tag{26}$$

with Δ denoting the difference operator, υ the adjustment matrix, b the observation number, $\mathcal{P}$ the short-run adjustments, and $\mathcal{E}$ a white noise process. A rigorous explanation on how to compute β is outside the scope of the present paper, so the reader is referred to [16] for such details. We note that the order/number of lags of the VECM model used in the present example is set to 13, which is found by using the method proposed by Dao et al. [44].

The obtained cointegration residual can be seen in Fig. 8a, and the associated ROC curve is depicted in Fig. 8b. From Fig. 8a, we can see that no clear decision boundary is present between the undamaged and damaged states, hence leading to rather poor damage detection results with FPR = 0.246, TPR = 0.710, AUC = 0.785, and Acc = 0.736. When comparing these statistics with the ones obtained using the proposed CL scheme, see Tb. 3, it is evident that the proposed scheme outperforms the cointegration-based method.

6. Conclusion

This paper proposes a new scheme for dealing with the effect of temperature variability in vibration-based damage detection. The scheme employs CL mode shapes as features that are designed to offer adequate sensitivity to damage and robustness to temperature variability. The design is performed by a proposed eigenvector assignment scheme, which is formulated as a bi-objective optimization problem. The first objective expresses the reciprocal of the sensitivity to damage and is to be

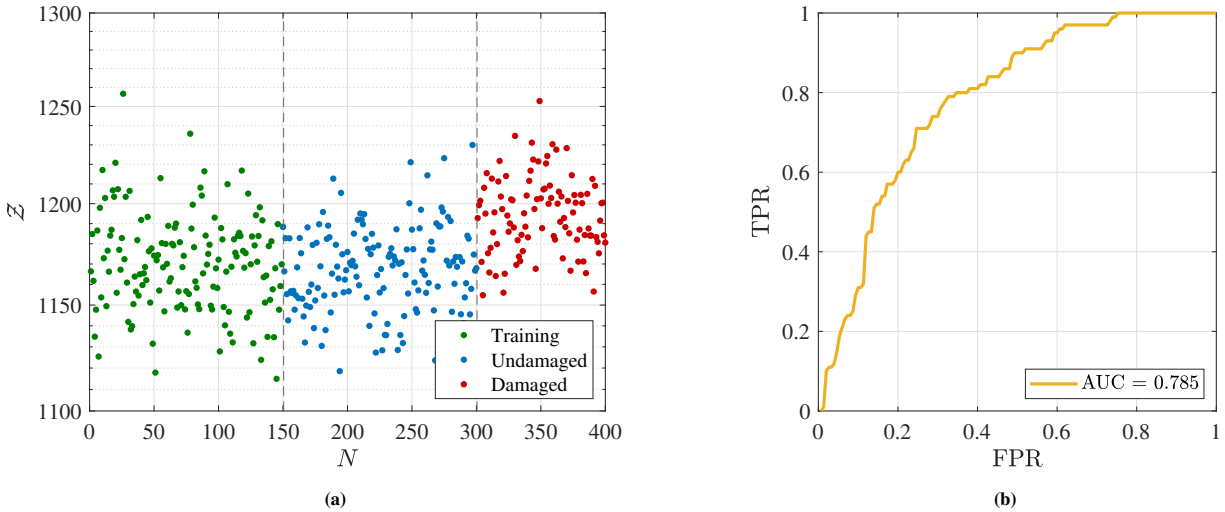

Fig. 8: Damage detection results for damage case 2 with (a) showing the cointegration residual and (b) the associated ROC curve.

minimized. The second objective is a measure of the linear independence between the real and imaginary parts of the assigned CL mode shapes, which quantifies the CL damping model's deviation from a classical distribution in the assigned modes. As classically damped mode shapes are invariant to spatially uniform stiffness changes, the latter objective is minimized to promote robustness to temperature variability.

The proposed CL scheme is tested on the basis of an illustrative example with a chain system and a 2-story frame structure model; both systems exposed to temperature variability. We see that the CL scheme effectively enhances the sensitivity to damage of the selected mode shapes while preserving adequate robustness to temperature variability, hence leading to good damage detectability. Finally, the scheme is compared to a well-established method for mitigating the effect of temperature variability, namely, cointegration in the context of the frame structure. To this end, it is seen how the CL scheme outperforms the cointegration-based method.

References

[1] C. R. Farrar, K. Worden, Structural health monitoring: A machine learning perspective, 1st Edition, John Wiley & Sons, Inc., 2013.

[2] M. D. Ulriksen, Damage localization for structural health monitoring: An exploration of three new vibration-based schemes, Ph.D. thesis, Aalborg University, Aalborg, Denmark (2018).

[3] S. Doebling, C. Farrar, M. Prime, A summary review of vibration-based damage identification methods, The Shock and Vibration Digest 30 (1998) 91–105. doi:10.1177/058310249803000201.

[4] H. Sohn, M. Dzwonczyk, E. G. Straser, A. S. Kiremidjian, K. H. Law, T. Meng, An experimental study of temperature effect on modal parameters of the alamosa canyon bridge, Earthquake Engineering & Structural Dynamics 28 (8) (1999) 879–897. doi:10.1002/(SICI)1096-9845(199908)28:8<879::AID-EQE845>3.0.CO;2-V.

[5] B. Peeters, G. De Roeck, One-year monitoring of the z24-bridge: environmental effects versus damage events, Earthquake Engineering & Structural Dynamics 30 (2) (2001) 149–171. doi:10.1002/1096-9845(200102)30:2<149::AID-EQE1>3.0.CO;2-Z.

[6] T. Bull, M. D. Ulriksen, D. Tcherniak, The effect of environmental and operational variabilities on damage detection in wind turbine blades, in: Proceedings of the 9th European Workshop on Structural Health Monitoring (EWSHM), Manchester, UK, 2018, pp. 1–9.

[7] E. J. Cross, On structural health monitoring in changing environmental and operational conditions, Ph.D. thesis, The University Of Sheffield, Sheffield, England (2012).

[8] M. D. H. Bhuyan, G. Gautier, N. Le Touz, M. Döhler, F. Hille, J. Dumoulin, L. Mevel, Vibration-based damage localization with load vectors under temperature changes, Structural Control and Health Monitoring 26 (11) (2019) e2439. doi:10.1002/stc.2439.

[9] R. Hou, X. Wang, Q. Xia, Y. Xia, Sparse bayesian learning for structural damage detection under varying temperature conditions, Mechanical Systems and Signal Processing 145 (2020) 106965. doi:10.1016/j.ymssp.2020.106965.

[10] B. A. Qadri, L. D. Avendaño-Valencia, J.-O. Hooghoudt, D. Tcherniak, M. D. Ulriksen, Removal of environmental and operational effects in damage detection: A comparative study with an operating wind turbine, Structural health monitoring(submitted) (2020).

[11] I. Jolliffe, Principal Component Analysis, Springer Verlag, 1986.

[12] A.-M. Yan, G. Kerschen, P. De Boe, J.-C. Golinval, Structural damage diagnosis under varying environmental conditions - Part I: A linear analysis, Mechanical Systems and Signal Processing 19 (2005) 847–864. doi:10.1016/j.ymssp.2004.12.002.

[13] A. D. F. Santos, M. F. M. Silva, C. S. Sales, J. C. W. A. Costa, E. Figueiredo, Applicability of linear and nonlinear principal component analysis for damage detection, in: 2015 IEEE International Instrumentation and Measurement Technology Conference (I2MTC) Proceedings, 2015, pp. 869–874.

[14] A. Deraemaeker, K. Worden, A comparison of linear approaches to filter out environmental effects in structural health monitoring, Mechanical Systems and Signal Processing 105 (2018) 1–15. doi:https://doi.org/10.1016/j.ymssp.2017.11.045.

[15] R. Engle, C. Granger, Co-integration and error correction: Representation, estimation, and testing, Econometrica 55 (2) (1987) 251–276.

[16] E. J. Cross, K. Worden, Q. Chen, Cointegration: a novel approach for the removal of environmental trends in structural health monitoring data, Proceedings of the Royal Society A: Mathematical, Physical and Engineering Sciences 467 (2133) (2011) 2712–2732. doi:10.1098/rspa.2011.0023.

[17] E. J. Cross, K. Worden, Approaches to nonlinear cointegration with a view towards applications in SHM, Journal of Physics: Conference Series 305 (2011) 012069. doi:10.1088/1742-6596/305/1/012069.

[18] P. B. Dao, Cointegration method for temperature effect removal in damage detection based on lamb waves, Diagnostyka Vol. 14, No. 3 (2013) 61–67.

[19] P. B. Dao, W. J. Staszewski, Data normalisation for lamb wave–based damage detection using cointegration: A case study with single- and multiple-temperature trends, Journal of Intelligent Material Systems and Structures 25 (7) (2014) 845–857. doi:10.1177/1045389X13512186.

[20] B. A. Qadri, M. D. Ulriksen, L. Damkilde, D. Tcherniak, Cointegration for detecting structural blade damage in an operating wind turbine: An experimental study, in: S. Pakzad (Ed.), Dynamics of Civil Structures, Volume 2: Proceedings of the 37th IMAC, A Conference and Exposition on Structural Dynamics 2019, Springer International Publishing, 2020, pp. 173–180. doi:10.1007/978-3-030-12115-0_23.

[21] M. D. Spiridonakos, E. N. Chatzi, Metamodeling of dynamic nonlinear structural systems through polynomial chaos narx models, Computers & Structures 157 (2015) 99–113. doi:10.1016/j.compstruc.2015.05.002.

[22] L. D. Avendaño-Valencia, E. N. Chatzi, K. Y. Koo, J. M. W. Brownjohn, Gaussian process time-series models for structures under operational variability, Frontiers in Built Environment 3 (2017) 1–19. doi:10.3389/fbuil.2017.00069.

[23] K. Tatsis, V. Dertimanis, Y. Ou, E. N. Chatzi, Gp-arx-based structural damage detection and localization under varying environmental conditions, Journal of Sensor and Actuator Networks 9 (3) (2020) 41. doi:10.3390/jsan9030041.

[24] L. D. Avendaño-Valencia, E. N. Chatzi, D. Tcherniak, Gaussian process models for mitigation of operational variability in the structural health monitoring of wind turbines, Mechanical Systems and Signal Processing 142 (2020) Article – 106686. doi:10.1016/j.ymssp.2020.106686.

[25] L. R. Ray, L. Tian, Damage detection in smart structures through sensitivity enhancing feedback control, Journal of Sound and Vibration 227 (5) (1999) 987–1002. doi:https://doi.org/10.1006/jsvi.1999.2392.

[26] D. Bernal, M. D. Ulriksen, Output feedback in the design of eigenstructures for enhanced sensitivity, Mechanical Systems and Signal Processing 112 (2018) 22–30. doi:10.1016/j.ymssp.2018.04.032.

[27] M. D. Ulriksen, D. Bernal, On the use of complex gains in virtual feedback for model updating, in: International Conference on Structural Engineering Dynamics (ICEDyn), 2019, pp. 1–7.

[28] L. J. Jiang, J. J. Tang, K. W. Wang, An optimal sensitivity-enhancing feedback control approach via eigenstructure assignment for structural damage identification, Journal of Vibration and Acoustics 129 (6) (2007) 771–783. doi:10.1115/1.2748476.

[29] K. Worden, C. R. Farrar, G. Manson, G. Park, The fundamental axioms of structural health monitoring, Proceedings of the Royal Society A: Mathematical, Physical and Engineering Sciences 463 (2082) (2007) 1639–1664. doi:10.1098/rspa.2007.1834.

[30] P. C. Mahalanobis, On the generalised distance in statistics, Proceedings of the The National Institute of Science of India 2 (1) (1936) 49–55.
[31] T. K. Caughey, Classical normal modes in damped linear dynamic systems, Journal of Applied Mechanics 27 (2) (1960) 269–271. doi:10.1115/1.3643949.
[32] J. M. W. Brownjohn, T. C. Pan, H. K. Cheong, Dynamic response of republic plaza, singapore, The Structural Engineer 76 (11) (1998) 221–226.
[33] F. Magalhães, E. Caetano, Álvaro Cunha, Operational modal analysis and finite element model correlation of the braga stadium suspended roof, Engineering Structures 30 (6) (2008) 1688–1698. doi:10.1016/j.engstruct.2007.11.010.
[34] C. Gentile, A. Saisi, Operational modal testing of historic structures at different levels of excitation, Construction and Building Materials 48 (2013) 1273–1285. doi:10.1016/j.conbuildmat.2013.01.013.
[35] P. Van Overschee, B. De Moor, Subspace identification for linear systems. Theory, implementation, applications, Kluwer Academic Publishers Group, 1996. doi:10.1007/978-1-4613-0465-4.
[36] M. D. Ulriksen, Closed-loop model updating for damage isolation in structural systems exposed to temperature variability, Applied Mathematical Modelling(to appear) (2021).
[37] R. B. Nelson, Simplified calculation of eigenvector derivatives, AIAA Journal 14 (9) (1976) 1201–1205. doi:10.2514/3.7211.
[38] A. H. Al-Mohy, N. J. Higham, The complex step approximation to the fréchet derivative of a matrix function, Numerical Algorithms 53 (2010) 133–148. doi:10.1007/s11075-009-9323-y.
[39] S. Gass, T. Saaty, The computational algorithm for the parametric objective function, Naval Research Logistics Quarterly 2 (1-2) (1955) 39–45. doi:10.1002/nav.3800020106.
[40] Y. Y. Haimes, L. S. Lasdon, D. A. Wismer, On a bicriterion formulation of the problems of integrated system identification and system optimization, IEEE Transactions on Systems, Man, and Cybernetics SMC-1 (3) (1971) 296–297. doi:10.1109/TSMC.1971.4308298.
[41] K. Deb, Multi-Objective Optimization using Evolutionary Algorithms, John Wiley & Sons, Inc., 2001.
[42] J. P. Egan, Signal detection theory and ROC-analysis, Academic Press, 1975.
[43] S. Johansen, Statistical analysis of cointegration vectors, Journal of Economic Dynamics and Control 12 (2) (1988) 231–254. doi:https://doi.org/10.1016/0165-1889(88)90041-3.
[44] P. B. Dao, W. J. Staszewski, A. Klepka, Stationarity-based approach for the selection of lag length in cointegration analysis used for structural damage detection, Computer-Aided Civil and Infrastructure Engineering 32 (2) (2017) 138–153. doi:10.1111/mice.12238.